Check for updates

# Monte Carlo simulation of a LSC based on stacked layers of fiber arrays with core-coating different absorbing properties

R. BARCIELA,[1,2] F. QUINTERO,[1,2,*] A. F. DOVAL,[1] M. FERNÁNDEZ-ARIAS,[1,2] J. DEL VAL,[2,3] R. COMESAÑA,[2,4] AND J. POU[1,2]

[1]*Applied Physics Department, Universidade de Vigo, E.E.I., 36310 Vigo, Spain*
[2]*CINTECX, Universidade de Vigo, LaserON research group, E.E.I., 36310 Vigo, Spain*
[3]*Centro Universitario de la Defensa, Escuela Naval Militar, Plaza de España 2, 36920 Marín, Spain*
[4]*Materials Engineering Dpt., University of Vigo, EEI, Lagoas-Marcosende, Vigo, 36310, Spain*
[*]*fquintero@uvigo.es*

**Abstract:** In this work, a Monte Carlo ray-tracing model for the simulation and optimization of a fiber Luminescent Solar Concentrator (LSC) based on stacked layers of fiber arrays is developed and validated. The fiber LSC efficiency improvements are compared against a conventional planar LSC. We developed a new model to analyze the performance of different configurations of bulk-doped fibers and fibers constituted by a doped coating and a passive core. These configurations are analyzed also varying fiber packing geometry diameters, and length. Due to the exceptionally low absorption coefficient of the silica fibers ($\alpha_{wg} \approx 10^{-4}$ cm$^{-1}$), concentration factors of up to 1.9 are predicted when dimensions are scaled over 1 m$^2$, which improve more than twice the maximum concentration factor ever reported. These results serve as a preliminary theoretical study for the future development of a new LSC design based on flexible silica micro-fibers coated with Si-QDs doped poly(lauryl methacrylate) (PLMA) layers.

## 1. Introduction

The need to replace fossil fuels by less pollutant and renewable energy sources is a priority in order to carry out the energy transition. To this end, photovoltaic energy is one of the most encouraging alternatives, since it is estimated that the solar radiation received by the Earth in an hour equals the global energy consumption in a year [1]. Continuous improvements in solar devices have raised the efficiency of most silicon photovoltaic (PV) cells available on the market, ranging from 20% up to 25% [2]. However, silicon cells, both crystalline (c-Si) and amorphous (a-Si), with an energy band gap $E_g$ = 1.1 eV, show a decrease of the spectral response outside the visible/near infrared (NIR) region (450 to 1000 nm), and it is widely recognized that solar devices performance can barely increase, as the theoretical maximum conversion efficiency for a single junction p-n silicon solar cell is capped at around 30% [3].

Unfortunately, despite such efficiency boosts, conventional "one sun" devices still have low generations as a result of the high solar flux dispersion, leading to the need for large PV panels, with their subsequent environmental impact. To face this issue, luminescent solar concentrators (LSCs) have been developed since 1976 [4] as a new solution for concentrating the naturally disperse and discontinuous solar flux.

An LSC consists of a semi-transparent matrix doped with a luminescent material which captures the incident radiation on a large sun-facing area by means of their dopants and re-emits it at a longer wavelength [5]. The matrix guides the re-emitted light by total internal reflection (TIR) towards the edges, where a PV cell is attached. Due to the large difference between the area of the exposed surface to that of its edges, LSCs work as solar concentrators, replacing

the large, expensive PV panels by a cost-effective waveguide material. Furthermore, the use of suitable doping particles into the matrix acting as spectral converters makes viable their coupling to high quality cells with a higher external quantum efficiency (EQE) in a narrower window of performance (500 to 800 nm), since the absorption-emission process of the luminescent material transform the solar spectrum to match the spectral characteristics of the photovoltaic material. This is the case, for example, of thin film chalcogenide cells (e.g., copper indium gallium selenide (CIGS) and copper zinc tin sulfide (CZTS)) [6].

Additional advantages can be highlighted, such as the low sensitivity to the radiation angle, allowing for a high efficiency in diffused, indirect light conditions [7], and their transparency, which allows the integration into windows, facades or roofs without interfering with the lighting of the space. Thus, they represent a great advance in the installation of so-called zero energy buildings.

LSC performance is commonly quantified by means of the optical efficiency. A common definition is optical efficiency of photon flux $\eta_{op}$, defined as [8] :

$$\eta_{op} = \frac{\Phi_{p2}}{\Phi_{p1}} \tag{1}$$

Where $\Phi_{p1}$ is the incident photon flux in the exposed area and $\Phi_{p2}$ is the collected photon flux at the LSC/PV cell boundary.

In a similar way, the optical efficiency of radiant power $\eta_{oe}$ is defined as:

$$\eta_{oe} = \frac{\Phi_{e2}}{\Phi_{e1}} \tag{2}$$

Where $\Phi_{e1}$ is the incident radiant power in the exposed area and $\Phi_{e2}$ is the collected radiant power at the LSC/PV cell boundary.

In case of a monochromatic source, since collected photons are usually down-shifted to longer wavelengths by the embedded dopants, $\eta_{oe}$ is lower than $\eta_{op}$ by a factor given by the Stokes efficiency $\eta_s$ :

$$\eta_s = \frac{\eta_{oe}}{\eta_{op}} = \frac{\overline{\lambda}_1}{\overline{\lambda}_2} \tag{3}$$

Where $\overline{\lambda}_1$ and $\overline{\lambda}_2$ are the mean wavelength of the incident and collected photons, respectively. The radiant power concentration factor $C_{oe}$ is defined as the ratio of the incident radiant power density $\Phi_{e1}/A_1$ at the exposed area $A_1$ to the collected radiant power density $\Phi_{e2}/A_2$ at the cell area $A_2$. $C_{oe}$ factor is related to the optical efficiency $\eta_{oe}$ by the geometric gain factor $G = A_1/A_2$:

$$C_{oe} = \eta_{oe} G \tag{4}$$

The $C_{oe}$ factor is conceived as the effective increase of PV cell area when a certain area of PV material exposed to radiation is replaced by an LSC with the same exposed area. For concentration aims, $C_{oe}$ must be greater than unity. Otherwise, when $C_{oe} < 1$, it means the same area of PV cell would receive less power when attached to the LSC than directly exposed to sun light. However, even in this case, a greater performance is possible when selecting PV cell spectrally-matched doping particles, thus compensating a poor $C_{oe}$ factor with a high PV energy conversion efficiency.

Typical state-of-the-art LSCs have similar dimensions (around several centimeters) and $G$ values, so their performance is typically quantified based on efficiencies. So far, the best obtained efficiencies are still low. The largest values reported for flat single-layer LSCs without external devices (e.g. mirrors and white diffusers) where achieved for a 12 cm × 12 cm × 0.26 cm Si quantum dots (QDs) LSC ($\eta_{oe}$ = 2.85%) [9] and 12 cm × 12 cm × 0.3 cm CuInSe2/ZnS QDs

LSC ($\eta_{oe}$ = 3.27%) [10], both based on a poly(lauryl methacrylate) (PLMA) host matrix. While the maximum $\eta_{oe}$ value ever reported for a LSC without mirrors was reached with a cylindrical geometry consisting of a hollow PMMA fiber filled with a luminescent center of di-ureasil doped with Rh6G, with a value of 8% [11].

However, the integration of LSCs in structural elements requires their scaling up to several meters, resulting in a high geometric factor. In this case, the high $G$ factor may lead to high $C_{oe}$ achievements despite the expected optical efficiencies may be lower by one or two orders of magnitude than those of the centimeter-sized LSC. Consequently, the $C_{oe}$ factor is more representative of LSC performance in real applications. Unfortunately, for flat single-layer short-length LSCs, the highest $C_{oe}$ values attained considering the total spectral irradiance on Earth are not higher than 0.5 while the maximum concentration factor ever achieved reaches 0.9 [11].

The low efficiencies and limited dimensions of the currently available LSCs are due to a number of loss mechanisms. For a better understanding of this losses, LSC optical efficiency can be expressed as [5]:

$$\eta_{op} = \eta_{abs}\eta_{col} \tag{5}$$

Where $\eta_{abs}$ is the absorption efficiency (the fraction of the incident photon flux harvested by the LSC dopants). It involves all losses affecting incident light before the first absorption event. They include external reflection losses of incident light at the LSC surface, host absorption losses and transmission losses of incident light, resulting from the limited optical density of the dopants.

$\eta_{col}$ is the collection efficiency (fraction of the absorbed flux reaching the PV cell). It involves all losses affecting incident light after the first absorption event. In this step, three main losses are involved: first are losses due to non-radiative energy processes resulting from the non-unity emission quantum yield, $\eta_{PL}$, of dopants. Second, losses due to re-emitted light reaching the host-air interface with an incidence angle lower than the critical angle $\theta_c$ = arcsin (1/$n$) such that no total internal reflection (TIR) takes place, these are denoted as escaping losses. Third, self-absorption of re-emitted photons by the dopants (which can be followed by non-radiative processes or re-emission with an angle lower than the critical angle). Finally, the fourth are parasitic waveguide losses caused by scattering from QDs and optical imperfections in the polymeric host.

Thus, in centimeter sized LSCs, self-absorption losses are the main factor limiting LSCs efficiency and a lot of studies tackled this issue to improve device performance [12,13]. In order to enhance incident light harvesting while minimizing self-absorption losses, ideal dopants requirements involve a high quantum yield $\eta_{PL}$ and a stepwise absorption profile $\alpha_d$ ($\lambda$) with a large absorption coefficient at shorter wavelengths (UV/VIS) and low absorption coefficients at the emission band.

However, when scaling-up LSC dimensions, host absorption becomes an additional loss mechanism limiting critically the realization of high-performance practical devices. State-of-the-art waveguide materials commonly used in LSCs are polymers such as soda-lime glass ($\alpha_{wg} \approx 0.5$ cm$^{-1}$), poly(methyl methacrylate) (PMMA) ($\alpha_{wg} \approx 3 \times 10^{-2}$ cm$^{-1}$), fluorinated PMMA ($\alpha_{wg} \approx 2 \times 10^{-4}$ cm$^{-1}$) or N-BK7 glass ($\alpha_{wg} \approx 1 \times 10^{-3}$ cm$^{-1}$) [5,14]. As an example, a marked attenuation produced by soda-lime glass or PMMA due to absorption in the waveguide involves a dramatic drop of efficiency of 80% and 50%, respectively, in just a few tens of centimeters [14]. So the introduction of host materials with high optical quality is one of the challenges for the development of practical devices.

Other losses decreasing the LSC performance at large areas are scattering losses, since the deviation of the propagation directions of the guided photons leads to an increase of the number of photons reaching the interfaces within the escape cone, resulting in higher loss probability [15]. Despite scattering theoretically shows a linear increase with QD concentration, this effect raises drastically in case of QD agglomeration [16–18] As an example, a scattering coefficient

$\alpha_{sc}$ as high as $3 \times 10^{-1}$ cm$^{-1}$ was reported for 0.1 wt% ester Si-QDs due to the presence of QDs clumps [17], which is around two orders of magnitude of the theoretical value of $2.5 \times 10^{-3}$ cm$^{-1}$ for Si-QDs with a diameter of 5 nm [16].

On the other hand, for applications in large area LSCs, cylindrical geometry has more advantages with respect to flat geometry due to its compatibility with optical fibers, being lighter, flexible and cost-effective. Apart from mechanical advantages, some theoretical studies revealed a better optical performance of fiber LSCs when comparing cylindrical and planar LSCs using ray-tracing techniques [19]. Specifically, the results highlighted lower reflection losses for an array of cylinders than a flat LSC and an optical concentration of a cylindrical LSC up to 1.9 times that of square-planar LSC. Additionally, a better performance was obtained for coated fibers than homogenously doped ones due to the higher trapping efficiency when emission occurs close to the surface.

Computational modelling is recognized as a time and cost-effective resource to orientate new LSC devices. Diverse approaches for LSC modeling can be found in the literature. Some works use LSC analytical models which may be useful for planar LSC shapes [4,7,20,21], but their complexity increases when changing LSC geometry [19,22]. Also, existing thermodynamic models, despite being fast and precise deterministic models, are also restricted to planar shapes [23,24]. Consequently, most of the available works use Monte Carlo ray-tracing models due to their simplicity and flexibility against alternative geometries [25,26]. Some of them attempt to model LSCs based on a single layer of fiber arrays [27–29]. However, there are no works that model multiple layers.

In this work, we develop a Monte Carlo ray-tracing model of solar radiation absorption, emission and reabsorption in the luminophores, as well as waveguiding, in order to analyze the performance of a novel LSC design consisting of stacked layers of fiber arrays. The model is firstly designed and validated for a planar LSC and then it is applied to a cylindrical geometry.

The fiber LSC efficiency improvements are compared against a conventional planar LSC while varying some parameters of interest such as the fiber packing geometry, diameter, length, dopants distribution (homogeneously doped or coated) or coating thickness.

This work serves as a previous theoretical study for the future development of a new LSC design based on flexible silica micro-fibers coated with Si-QDs doped PLMA layers. The exceptionally low absorption coefficient of the silica fibers ($\alpha_{wg} \approx 10^{-4}$ cm$^{-1}$) is expected to reduce significantly the host absorption impact on the LSC performance on the contrast to the traditional polymer fibers when LSC dimensions are scaled over 1 m$^2$, leading to the highest concentration factors ever reported.

## 2. LSC description

The proposed LSC geometry consists of a square LSC based on stacked layers of fiber arrays (Fig. 1(a)). The fiber LSC is compared against a conventional square-planar LSC with the same volume of host material and exposed area $L^2$ (Fig. 1(b)). Different sets of fibers varying the external diameter, $D_e$, of the fibers are studied. For each diameter, the number of array layers is selected given the planar LSC thickness $w$, using relation from Eq. (6), thus ensuring the total fiber array volume is almost the same as the planar one.

$$N = \frac{4w}{\pi D_e} \tag{6}$$

Two types of fiber packings are considered: square packing (Fig. 1(c)) and hexagonal packing (Fig. 1(d)). Hexagonal packing (packing density of $\pi/\sqrt{12}$ is denser than square one (packing density of $\pi/4$). Following the approach reported in [19], the PV cells bound the four edges of the square-planar LSC while in the fiber array only the ending sides of the fibers are covered. In such conditions, fiber geometric factor $G_{cyl}$ doubles the geometric factor $G_{sq}$ of planar one.

The LSC materials analyzed in this work are composed of a solid host or matrix (PLMA) doped with silicon nanocrystals as the active layer, and un-doped PLMA or pure silica as passive waveguiding medium. The fibers can be either homogeneously doped (Fig. 1(e)) or coated (Fig. 1(f)). The coated fibers consist of a non-doped core of waveguiding material coated with a polymer doped layer. As shown in (Fig. 1(g)), the surface active layer has a higher dopant concentration compared to bulk-doped one, in order to have the same number of QDs per fiber length.
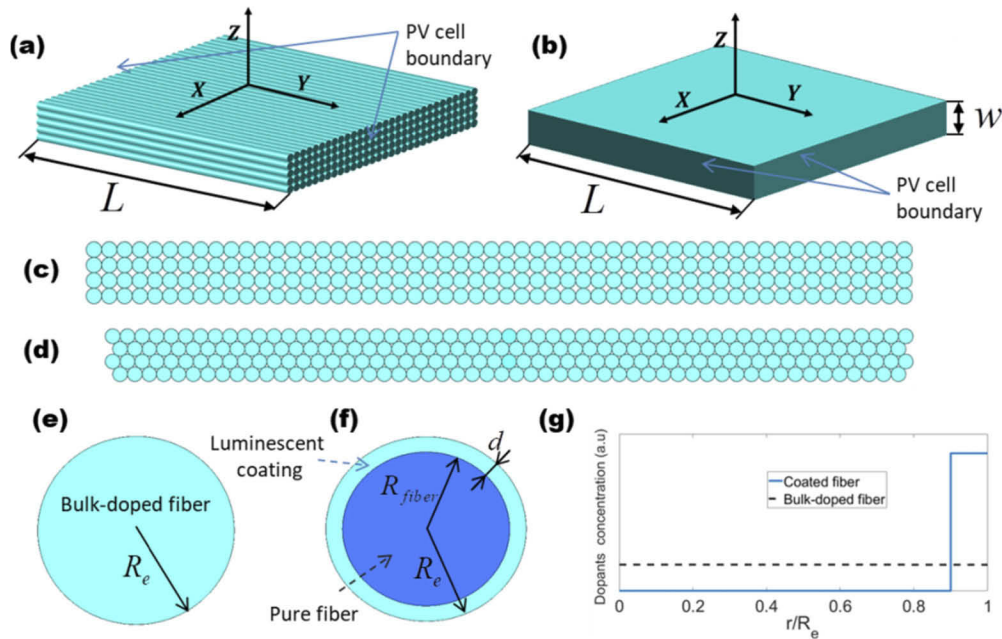


**Fig. 1.** (a) Square fiber LSC based on stacked layers of fiber arrays; (b) Square-planar LSC with an equivalent exposed area and volume; (c), (d) Fiber layers cross-sections of two fiber LSCs with square and hexagonal fiber packing; (e), (f) cross sections of bulk-doped and coated fibers; (g) Representation of dopants concentration redistribution in a coated fiber to keep the same number of dopants per fiber length.

The luminescent active material consists of a 0.09 wt% Si-QDs doped PLMA composite and their optical properties were taken from the optical characterization reported in [9]. Si-QDs, emitting at 830 nm, show a zero Stokes shift between the absorption and emission spectra, allowing to minimize self-absorption losses. The Si-QDs quantum yield is 46%. The PLMA background absorption measurements report a value around 0.02 cm$^{-1}$ in the VIS, reaching a peak 0.05 cm$^{-1}$ in the NIR (930 nm) due to the C–H vibration overtone. PLMA reported refractive index was 1.49.

In the first part of the study, coated fibers with a core waveguide of pure passive PLMA are considered. The efficiency of stacked layers of fiber arrays is compared against the square-planar LSC homogeneously doped with Si-QDs, designed for the same collection area $L^2$ and volume. Bulk-doped fibers with equivalent total diameter were also considered for comparison. The absorption efficiency was studied for different fiber diameters $D_{fiber}$ in order to study the light harvesting changes. Then, optical efficiency and concentration factor were calculated when the collection area is scaled up to more than 1 m$^2$ with the aim to estimate how PLMA fibers restrain the LSC performance at longer length scales.

In the second part, the inner PLMA fiber is replaced by a silica fiber. The Si-QDs concentration in the luminescent coating is increased to have the same absorption efficiency as the planar LSC. The optical efficiency and concentration factor are simulated again to see performance improvements respect to the LSC based on PLMA fibers.

## 3. Ray tracing model development

In this work, we develop a ray-tracing model of solar radiation absorption, emission and reabsorption in the luminophores, as well as waveguiding through the fibers. The model is firstly designed and validated for a planar LSC and then it is applied to a cylindrical geometry in order to model the design proposed. The flow diagram illustrating the general scheme of the Monte Carlo method employed for the simulation, Fig. S1, is presented in the Supplemental document (see Supplement 1).

Simulations involve discrete photons generated at wavelength intervals of 1 nm, each given the statistical weight according to the AM1.5G spectrum in terms of photon flux [30]. We assume the validity of the ray-tracing approximation since core diameter as well as coating thickness are reasonably larger than the wavelength of the fluorescence light, for all the simulated fibers, therefore behaving as multimode [31]. Particularly, the shortest simulated coating thickness and core diameter are around 4 and 36 times greater than emission wavelength of 830 nm. In addition, the spectral width of the fluorescent light is relatively large, and its coherence length, given by Eq. (7), is short enough to neglect any interference effect inside de fiber [32].

$$l_{coh} = \frac{\lambda^2}{n\Delta\lambda} \tag{7}$$

Where $\lambda$ is the emission wavelength, $\Delta\lambda$ spectral bandwidth and $n$ is the refractive index. Taking into account dopants guided light shows its peak emission at 830 nm with a full-width at half-maximum of 150 nm and an approximate refractive index value of 1.5, Eq. (7) yields a coherent length for the guided radiation $l_{coh} \approx 3$ μm which is 10 times lower than the shortest simulated diameter, so the interference effects can be neglected.

The ray interaction with an interface is modelled following an stochastic approach where the ray is not divided when reaching the interface. Instead, it can be either a reflected or a transmitted to the refractive media with a probability given by the reflectance calculated from Fresnel's laws for planar waves incident in a flat surface. The first condition is fulfilled as the solar radiation is sufficiently flat while the second one can be accepted when the fiber diameter is much larger than the wavelength of the guided light ($\approx 1$ μm).

In addition, we assume that Beer-Lambert law also applies to QDs concentration, and hence dopants absorption coefficient varies linearly with the dopant concentration in the host matrix. On the other hand, dopant concentrations are low enough to neglect the imaginary contribution of the refractive index $\tilde{n} = n(1 + i\kappa)$, which can be done when $\kappa$, given by Eq. (8) is, much lower than one [32].

$$\kappa = \frac{\lambda_0 \alpha_d}{4\pi n} << 1 \tag{8}$$

Where $\lambda_0$ is the wavelength of incident light, $\alpha_d$ the dopant decadic absorption coefficient and $n$ the host refractive index. Therefore the doped PLMA coating behaves as an imperfect dielectric.

In bulk-doped fibers, the fiber refractive index $n$ determines escaping losses as it defines the critical angle limiting TIR of the fluorescent photons during their propagation along the fiber. McIntosh *et al.* [19] shown in a theoretical study of cylindrical LSCs that the closer to the surface the fluorescent photons are emitted the higher the trapping efficiency is (i.e. a lower fraction of the emission directions lies inside de escape cone). As an example, for $n = 1.5$, trapping efficiency reaches a 74.5% when emission occurs close to the surface of the fiber in contrast with

only a 33.3% for emission in the center. For this reason, regarding escaping losses, coated fibers take advantage of homogenously doped ones, especially when coating thickness is reasonably thin.

On the other hand, for coated fibers, the relation between the inner core and coating refractive indexes, $n_i$ and $n_e$, respectively, plays a key role in the LSC performance as it determines some important losses mechanisms in the fiber [22]. Therefore, two cases are distinguished: $n_i > n_e$ and $n_i < n_e$. Both share the downside that the rays cannot be confined exclusively inside the inner core as it is not possible that rays emitted in the coating can be trapped by TIR at the core surface once they cross the internal interface to the core. However, $n_i > n_e$ condition takes the advantage that rays cannot be trapped in the high absorbing coating by TIR at the internal interface, therefore, reducing host losses. Instead, their paths consist of successive reflections at the external fiber interface, crossing the internal interface twice between each reflection. In contrast, when $n_i < n_e$, the existence of escape cone for emitted light at the internal interface implies a fraction of these rays to be guided exclusively inside the coating, and suffering high attenuation. Although, despite the waveguiding advantage of $n_i > n_e$ configuration, it has the downside of the lower refractive index $n_e$ of the coating, which increases the escaping losses at the external surface of the fiber with respect to a single undoped inner fiber with refractive index $n_i$. Conversely, when $n_i < n_e$, the higher refractive index $n_e$ of the coating reduces the escaping losses to the air.

With regards to QDs absorption, we consider that the optical path traveled by the beams is much greater than the dopants separation. Consequently, continuous nature of the dopant is assumed and hence Beer-Lambert law is applied for the generation of absorption optical path lengths. In such conditions, absorption effects by the different absorbers are modelled by generating random path lengths $\Delta s$ according to the inverse cumulative density function as Eq. (9), which the ray travels before absorption.

$$\Delta s = -\frac{log_{10}\xi}{\alpha(\lambda)} \tag{9}$$

Where $\alpha(\lambda)$ is the decadic absorption coefficient and $\xi$ is a random variable uniformly distributed from 0 to 1. Three different absorption path lengths are generated for the inner host material, the outer host material and the QDs according to their respective absorption coefficients, $\alpha_{h,i}$, $\alpha_{h,e}$ and $\alpha_d$, by generating three random independent $\xi$ values. The absorption occurs when the ray propagates all over any of the pathlengths generated.

In order to take into account the scattering effects at long lengths, a scattering probability is included and described in terms of a scattering coefficient $\alpha_{sc}$. Therefore, in the same manner as absorption, a scattering path length $\Delta s_{sc}$ is generated following Eq. (9), which the ray travels before scattering [16]. Once reaching a scattering center, the ray is deviated isotropically and a new scattering path length is generated in order to model successive scattering events. Once a ray is absorbed by a QD, it can be re-emitted isotropically or undergo a non-radiant process, with a probability given by the quantum efficiency of the dopant.

The emission wavelength of the dopant is generated by applying the rejection sampling method to the emission spectrum of the dopant. To ensure an energy photon down-shifting, it is also imposed that the emission wavelength must be greater than the absorption wavelength. Once the photon is re-emitted, subsequent absorption and scattering paths are generated at the down-shifted wavelength, thus given the possibility for the photon to be lost by QD self-absorption, host absorption or a scattering event. A perfect index matching is considered at the LSC-PV cell coupling, so all photons arriving the interface are supposed to be absorbed by the cell. A more comprehensive explanation of the Monte Carlo algorithm is presented in the Supplemental document (see Supplement 1). Also, the complete code for the simulation of a wide surface LSC composed of stacked layers of fiber arrays with doped coating and undoped core with different refractive index and absorbing properties can be accessed from Code 1 (Ref. [33]).

In Fig. 2 some random propagation paths resulting from the simulation of different incident photons in 2 cm long PLMA based single fibers are represented: a bulk-doped fiber with a diameter of 120 μm (Fig. 2(a)) and coated fibers based on a pure PLMA core and a Si-QDs doped PLMA coating with a core diameter of 100 μm and a coating thickness of 10 μm (Fig. 2(b),(c)). Simulated incident photons are absorbed and emitted isotropically by a dopant (blue dots) and then guided inside the fiber until they are collected by the PV cell (green dots). For bulk-doped fibers the light is guided along the fiber as long as the emitted photon direction is outside the escape cone (Fig. 2(a)). For PLMA coated fibers, since core refractive index equals the coating one, all re-emitted rays impinging on the internal interface, are transmitted to the core and follow a high ratio of their path along the pure PLMA core, as observed in Fig. 2(b). However, as Fig. 2(c) reveals, although $n_i < n_e$ condition is not fulfilled, there are still some photons which are confined in the coating. This fraction of photons are re-emitted with an angle nearly parallel to the surface and cannot reach the core-coating boundary and instead, must travel a long helical path along the doped coating, thus having a high probability to be re-absorbed.
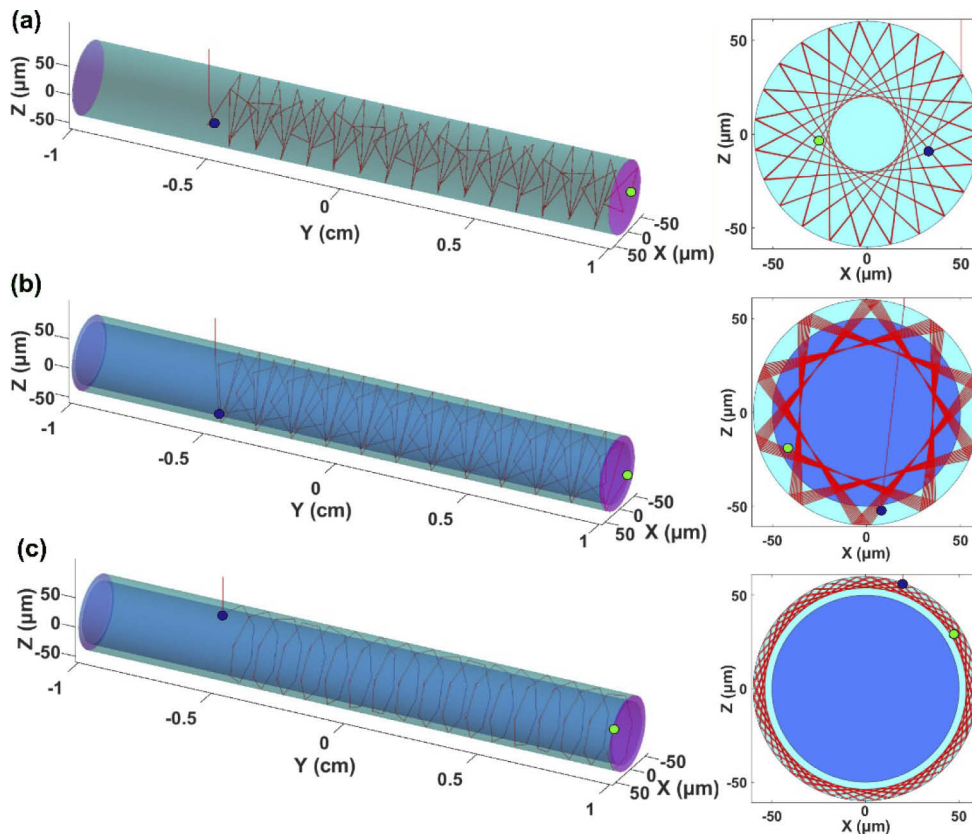


**Fig. 2.** Representation of some random propagation paths of different fluorescent photons after an absorption-emission event (blue dots) until collected at the PV cell (green dots) for 2 cm long PLMA based fibers: (a), bulk-doped PLMA fiber with a diameter of 120 μm and, (b), (c), coated fibers based on a pure PLMA core and a Si-QDs doped PLMA coating with a core diameter of 100 μm and a coating thickness of 10 μm. The *xz* projections of the paths are shown on the right. (b) Photon emitted in a direction such that a high ratio of the path is travelled through the inner medium. (c) Photon emitted in a direction such that the photon propagation is along the coating.

The use of a low-loss silica core can minimize the host losses of the core. Figure 3 presents some random propagation paths resulting from the simulation of different incident photons in silica fibers coated with a Si-QDs doped PLMA active layer. In this case, a high ratio of the fluorescent photons travel a great fraction of their total path inside the low-loss silica core and a substantially lower fraction along the high absorbing coating (Fig. 3(a),(b)). These paths result in lower ray-attenuation and may allow for a higher LSC performance. Meanwhile, the major host losses in silica fiber LSCs arise from rays confined in the coating following two different paths (Fig. 3(c),(d)). First path (Fig. 3(c)), is also observed in PLMA fibers (Fig. 3(c)), and involves rays emitted with a direction sufficiently parallel to the surface that they do not impinge on the internal interface, while the second one (Fig. 3(d)), arises from the slightly higher refractive index of the PLMA coating ($n_e$ = 1.49) with respect to the inner silica core one ($n_i$ = 1.45), which yields the possibility for re-emitted rays impinging on the internal interface to be confined within the coating by TIR. However, this additional path for absorption losses derived from the use of a coating material with a higher refractive index, could be balanced by the lower escaping losses of the coated fiber with respect to the uncoated silica one. Therefore, with the actual materials available, this is the optimal configuration, since we have an exceptionally low-loss core and a coating with a higher refractive index that enhances fluorescent light trapping along the fiber.

### 3.1. Validation

The model has been validated against experimental measurements on the Si-QDs doped PLMA planar LSC as reported by F. Meinardi *et al.* [9], with dimensions 12 cm × 12 cm × 0.26 cm and four Si solar cells attached to their edges. PLMA host and Si-QDs absorption coefficients were obtained from their respective absorption spectra, dividing them by the layer thickness, and they were fitted to both functions, $\alpha_{h,e}$ and $\alpha_d$, that model their wavelength dependence. Since there is no absorption data available in the UV, we assume that for wavelengths lower than the 350 nm threshold, LSC absorption is dominated by the QDs. Si-QDs emission spectra shape was modelled through a mix of three gaussian functions and the quantum yield was fixed to 46%.

In order to validate the model, a sample of $10^7$ incident photons from AM1.5G spectra was simulated and an histogram of the incident wavelengths grouped by the different events was represented for a clearer discussion (Fig. 4(a)). Results predict an absorption efficiency $\eta_{abs}$ of around 8% (region under black line), while the remaining 92% labelled as number 1, derived in losses due to surface reflections, light transparent to the matrix and around a 2% consisting of UV radiation below 350 nm absorbed by the PLMA host. Notwithstanding the apparently low absorption efficiency, this is not a worryingly unfavorable result if we consider that an ideal LSC must be transparent to visible light, and, ideally, it should absorb mainly UV radiation. The losses affecting the photons after being absorbed by the Si-QDs involve a 56% lost through non-radiative processes in first emission photons (#2), a 10.8% is lost by waveguide escaping (#3), a 8% is lost in the matrix host (#4) and a 1.25% is lost due to self absorption in the luminophores (#5). The remainder (#6) constitutes the collection efficiency, $\eta_{col}$. Taking into account Eq. (5), it is obtained an optical efficiency of photon flux of 1.95%. Considering the energy shift of the incident and collected photons (Eq. (3)), a simulated optical efficiency of radiant power of 2.65% is obtained. This result is almost equal to the value predicted in the simulations reported by Meinardi *et al.* [9], 2.67%, while also near to their experimental measurement of 2.85%. Considering only the absorbing region, a simulated $\eta_{op}$ value of 10.3% was estimated, while $\eta_{oe}$ is slightly lower (7.3%), in agreement with the energy down-shifting of the absorbed photons. The simulated collected spectra were also compared against the experimental results obtained in the work (Fig. 4(b)) when irradiating the LSC at two different spot distances ($d$ = 0 cm and $d$ = 12 cm). The simulated results have a similar tendency as seen in (Fig. 4(c)).
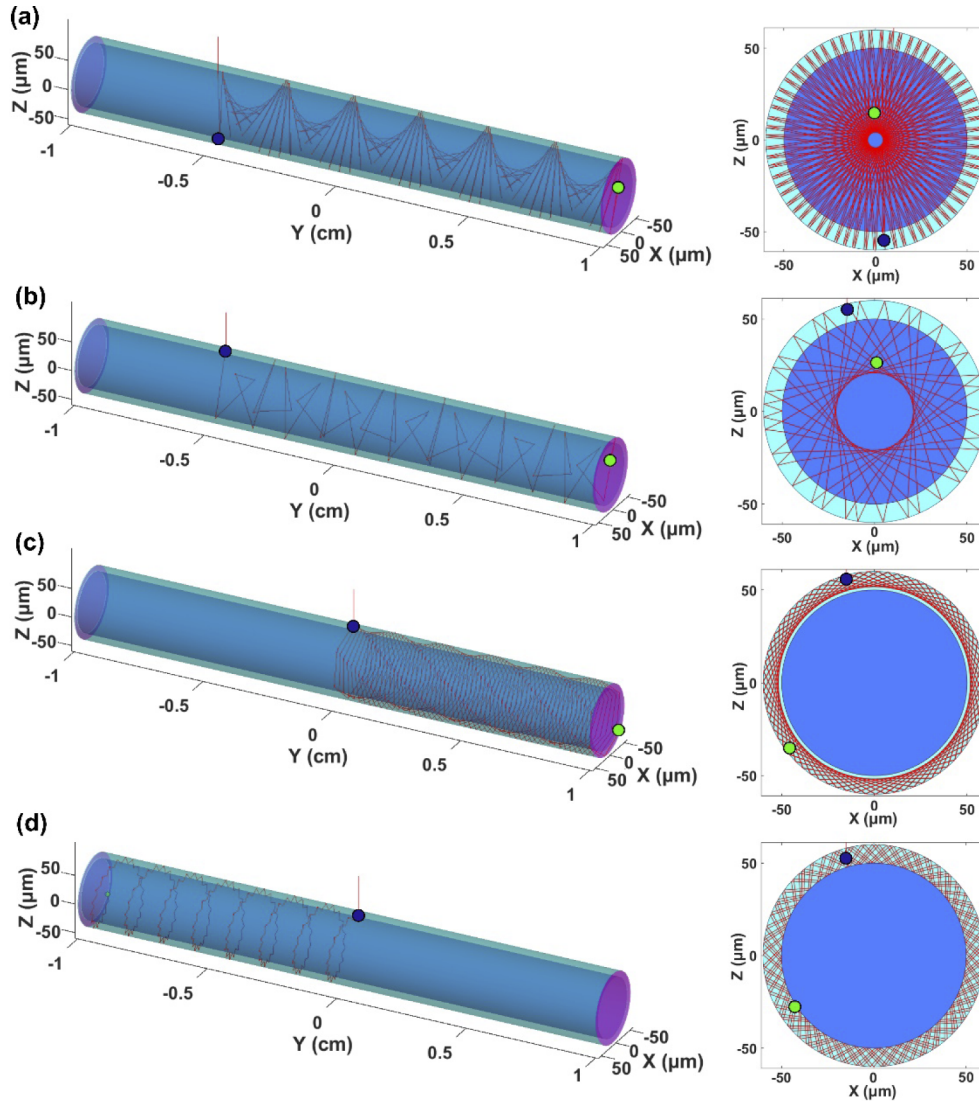
**Fig. 3.** Representation of some random propagation paths of different fluorescent photons after an absorption-emission event (blue dots) until collected at the PV cell (green dots) for 2 cm long fibers based on a pure silica core and a Si-QDs doped PLMA coating with a core diameter of 100 μm and a coating thickness of 10 μm. The *xz* projections of the paths are shown on the right. (a),(b), photons travelling a high ratio of the path through the silica low-loss medium. (c),(d) Photons propagated along the coating and resulting in a high attenuation.
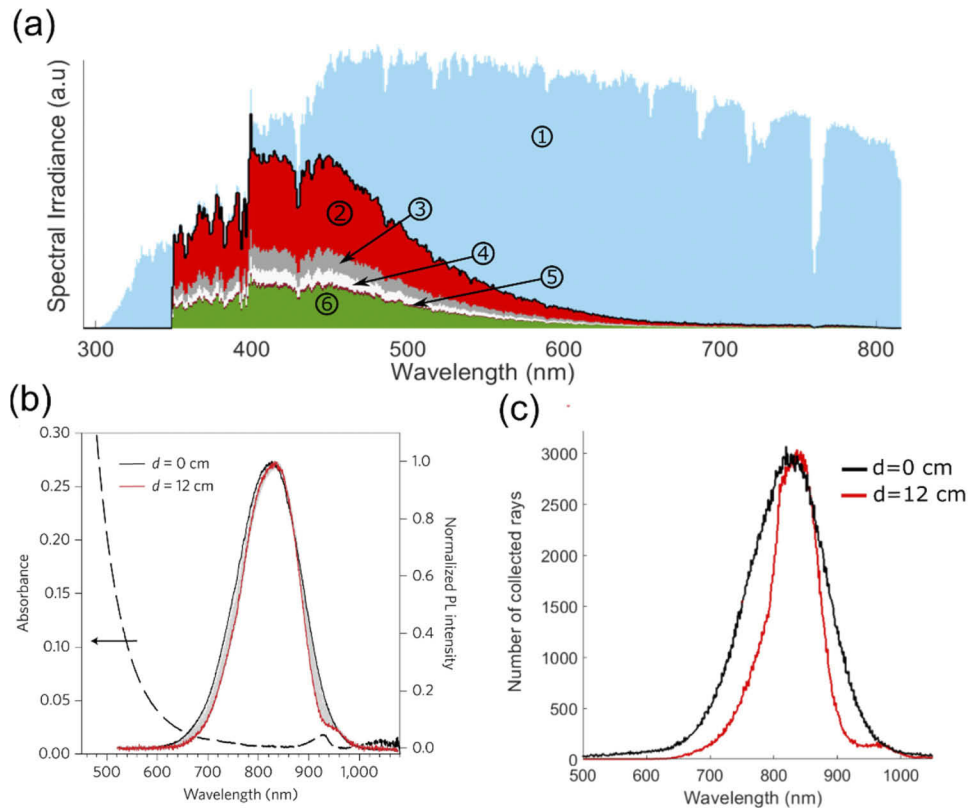
**Fig. 4.** (a) Histogram resulting from the simulation of a sample of $10^7$ incident photons from AM1.5G spectra. The region under the black solid line represents the fraction of the spectra absorbed by the QDs ($\eta_{abs} = 8\%$) while the region labelled as number 6 is the light collected by the PV cell ($\eta_{col} = 24.1\%$). The remaining regions represent the different losses affecting Si-QDs absorbed photons: a 56% of the absorbed light is lost through non-radiative processes in first emission photons (#2), a 10.8% corresponds to escaping losses (#3), a 8% is lost in the matrix host (#4) and a 1.25% is lost due to self-absorption in the QDs (#5). (b) Experimental spectra collected at the edge of the LSC when the excitation spot is located at different distances ($d = 0$ cm and $d = 12$ cm) from the edge. Reprinted by permission from Springer-Nature: Nature Photonics [9], Copyright 2017 Mcmillan Publishers Limited. (c) Histogram of the collected photons resulting from the simulation of the experiment described in (b) with the developed model.

## 4. PLMA inner fiber

Once the model was validated, it is applied to the proposed geometry of stacked layers of fiber arrays. In this part, a PLMA inner core is simulated. In order to study the absorption efficiency, different waveguide fiber diameters, $D_{\text{fiber}}$, were studied while the $d/D_{\text{fiber}}$ ratio was fixed to 0.1, with $d$ representing the thickness of the doped coating. Table 1 presents the diameter of the fibers analyzed, the resulting coating thickness, $d$, and total fiber diameter, $D_e$. The number of array layers for each diameter is estimated from Eq. (6) taking into account planar LSC thickness is 2.6 mm, to ensure a similar array volume as in [9].

**Table 1. Selected inner fiber diameters $D_{\text{fiber}}$ and the resulting coating thickness $d$, total diameter $D_e$ and the calculated number of layers $N_p$ to keep the same volume as a planar LSC. The selected number of layers $N$ are shown.**

| $D_{\text{fiber}}$ (µm) | $d$ (µm) | $D_e$ (µm) | $N_p$ (Eq. (6)) | $N$ |
|---|---|---|---|---|
| 2750 | 275 | 3300 | 1.003 | 1 |
| 1375 | 137.5 | 1650 | 2.006 | 2 |
| 600 | 60 | 720 | 4.598 | 5 |
| 200 | 20 | 240 | 13.79 | 14 |
| 100 | 10 | 120 | 27.59 | 28 |
| 60 | 6 | 72 | 45.98 | 46 |
| 30 | 3 | 36 | 91.96 | 92 |

For bulk-doped fibers, the dopant concentration was the same as reported by Meinardi *et al.* [9] (0.09 wt%) while for the coated fibers it was increased by a factor given by $D_e^2/(D_e^2 - D_{\text{fiber}}^2)$ in order to compensate the doped volume reduction and to include the same number of QDs in the total LSC. For $d/D_{\text{fiber}} = 0.1$ this relation yields a dopant concentration increase of 3.27, which means a 0.29 wt% total value. SiQDs decadic absorption coefficient $\alpha_d$ ($\lambda$) was increased proportionally to this change on dopant concentration.

Moreover, despite the frequently observed QD agglomeration accentuating scattering losses [17], the scattering modelling was done considering that the aim of this work is to make a prediction about the limiting performance for a Si-QDs based fiber LSC. Therefore, in this work, it is assumed that the Si-QDs are perfectly dispersed so that the only contribution is due to the isolated scattering centers. For this purpose, scattering coefficient was selected following calculations for single particle scattering performed by Hill *et al.* [16] obtaining a scattering coefficient $\alpha_{\text{sc}} \approx 2\times10^{-3}$ cm$^{-1}$ for 0.09 wt% QDs with a diameter of 4.3 nm. Additionally, for coated fibers, a linear relation of $\alpha_{\text{sc}}$ with QD concentration was assumed. Solar photons of different wavelengths sampled from solar AM1.5G spectrum are simulated at different points randomly distributed over the LSC surface. Normal incidence angle was selected simulating an AM1.5G source as in [9]. Additionally, an hemispherical light source modelling a diffuse incidence was included in the simulations to compare the fiber LSC performance against both types of light sources. Some examples of random paths of several simulated photons across two fiber LSCs with different fiber packing arrangements and diameters are presented in Fig. S2.

The absorption efficiency of bulk-doped and coated PLMA fiber LSCs for the fiber diameters reported in Table 1 with hexagonal and square fiber alignments are plotted in Fig. 5 under normal and diffuse incidence. Firstly, there is not an appreciable absorption efficiency variation between normal and diffuse incidence. In can be seen that coated fibers are less absorbing than bulk-doped fibers. Also, despite having the same number of QDs as planar geometry, incident light absorption is not the same as in the plane LSC, while also decreases for shorter fiber diameters. To explain this effect an histogram of the resulting path lengths $\Delta s$ (Fig. S3(a)) travelled by $10^6$ photons simulated in a bulk-doped 30 µm fiber LSC with hexagonal packing and their corresponding

absorption probability, according to $1 - 10^{-\alpha\Delta s}$ (Fig. S3(b)), are represented. Despite photons travel on average a longer absorption path length ($\overline{\Delta s}$ is higher than the planar LSC thickness $w$) the resulting average absorption is higher for the planar (fiber LSC mean absorption $\overline{A}$ is lower than the planar LSC absorption $A_{\text{p}}$) because of the high impact of photons travelling shorter distances on the absorption expression.
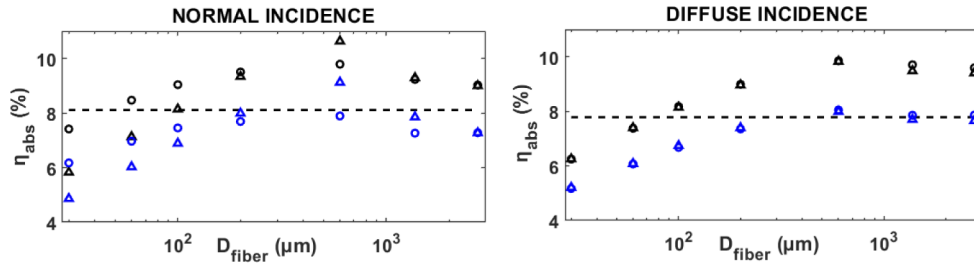


**Fig. 5.** Absorption efficiency of bulk-doped (black) and coated PLMA fiber LSCs (blue) with the fiber diameters reported in Table 1 with hexagonal (triangles) and square (circles) fiber alignments under normal and diffuse incidence. Dashed line represents absorption efficiency estimated for the planar LSC developed by Meinardi *et al.* [9].

On the other hand, these results show that under normal incidence the square fiber alignment is more absorbing than the hexagonal one, while under a diffuse source it is seen an invariance of absorption with the type fiber packing. In order to explain this, the mean path lengths $\overline{\Delta s}$ and number of interface interactions $N_{\text{int}}$ resulting from the simulation of fiber LSCs with different fiber diameters $D_{\text{fiber}}$ and the two fiber alignments, are shown in Table 2. Under direct incidence, it can be seen that square packed fiber simulations result in longer photon mean path lengths than hexagonal packed fiber ones. On the contrary, for diffuse incidence, path length results for both packing arrangements coincide each other. Additionally, it is noticed a slight path length increase with the diameter. Particularly, the path length increase reaches a 8% for fibers with a diameter of 200 μm compared with 30 μm ones.

**Table 2. Mean path lengths Δ$s$ and number of interface interactions $N_{\text{int}}$ resulting from the simulations of fiber LSCs with different fiber diameters and the two fiber alignments under direct and diffuse incidence.**

| | Direct normal incidence | | | | Diffuse (Lambertian) incidence | | | |
| | Hexagonal | | Square | | Hexagonal | | Square | |
| $D_{\text{fiber}}$ (μm) | $\overline{\Delta s}$ (cm) | $N_{\text{int}}$ | $\overline{\Delta s}$ (cm) | $N_{\text{int}}$ | $\overline{\Delta s}$ (cm) | $N_{\text{int}}$ | $\overline{\Delta s}$ (cm) | $N_{\text{int}}$ |
|---|---|---|---|---|---|---|---|---|
| 30 | 0.331 | 204 | 0.495 | 357 | 0.468 | 302 | 0.474 | 305 |
| 60 | 0.360 | 131 | 0.483 | 173 | 0.481 | 154 | 0.483 | 155 |
| 100 | 0.394 | 85 | 0.466 | 100 | 0.484 | 93 | 0.488 | 94 |
| 200 | 0.463 | 50 | 0.461 | 49 | 0.505 | 48 | 0.512 | 49 |

Collection efficiency is also evaluated to assess the performance of the design at longer dimensions, considering the four sources of losses affecting photons after the first absorption/emission process. For this purpose, the escaping losses, host losses, self-absorption losses and scattering losses are represented in Fig. 6 when varying the LSC length from 2 cm up to 5 m using fibers with a diameter of 30 μm and 3 μm of coating thickness, arranged in hexagonal and square packings and they are compared with the ones obtained from the simulation of the planar LSC developed by Meinardi *et al.* [9]. Since the resulting loss distribution of the new simulations for normal or diffuse incidence do not differ from each other, only losses for normal incidence are shown. First sight reveals that there is no significant influence of the fiber packing on the

collection losses. Secondly, major losses are due to photon escaping, which do not increase significantly as LSC length increases. The slight increase with length for shorter fibers arises from photons escaping from the fiber after the second absorption/emission event. On the other hand, host and self-absorption losses are low at lengths of a few centimeters, confirming the low PLMA absorption contribution at short lengths. However, when scaling-up LSC dimensions over one meter, due to the high Stokes shift of the Si-QDs, self-absorption losses become less important compared with host absorption losses, which show a dramatic impact improvement and achieve a similar contribution as escaping losses of more than a 20%. Additionally, scattering effects are the less influent losses, showing that it can be possible to reduce their impact on large LSCs performance by an adequate QD dispersion. Particularly, coated fibers bring the highest scattering losses due to their higher QD concentration required.
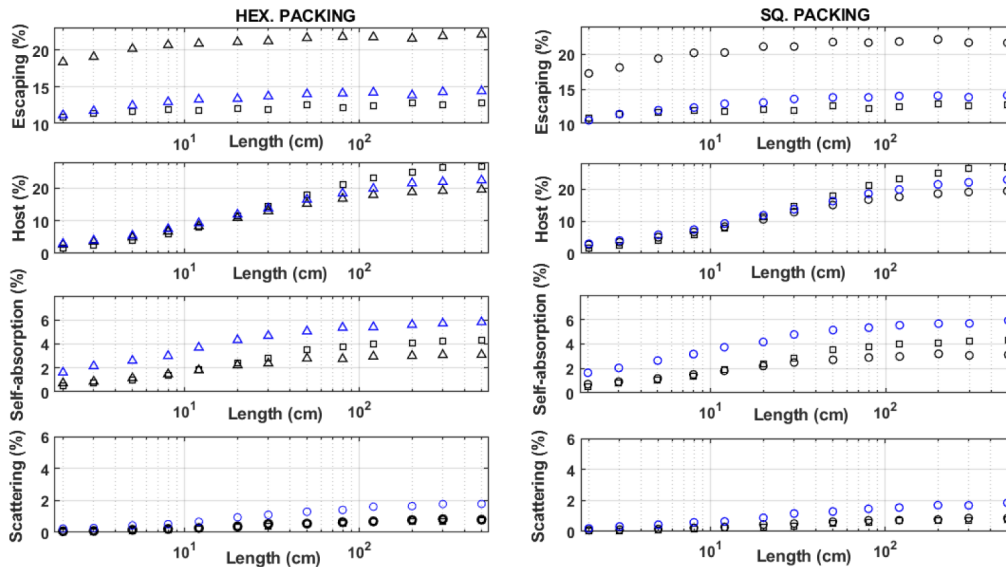


**Fig. 6.** The four sources of losses affecting photons after the first absorption/ emission process as a function of the LSC length for bulk-doped (black) and coated (blue) PLMA fibers with an inner diameter of 30 μm and 3 μm of coating thickness arranged in hexagonal (triangles) and square (circles) packings calculated for normal incidence. Squares represent losses estimated from the LSC developed by Meinardi *et al.* [9].

On the other hand, when comparing escaping and host losses of bulk-doped and coated fibers, some advantages and drawbacks can be noticeable. It is observed that in coated fibers escaping losses decrease with respect to that of the planar, as a result of the higher trapping efficiency when emission occurs at the surface. On the opposite, in bulk-doped fibers escaping losses remain higher. However, the positive effect of reduced escaping losses shown by coated fibers is balanced by their higher host losses. This is due to the higher fraction of guided rays (which result in a high absorption probability) and the long helical path the trapped rays have to travel through the fiber, therefore suffering more attenuation.

In Fig. 7, the optical efficiency $\eta_{oe}$ and concentration factor $C_{oe}$ as a function of the LSC length for bulk-doped and coated PLMA fibers are represented under normal and diffuse incidence and compared with the values estimated from the LSC developed by Meinardi *et al.* [9]. These results show that fiber LSC efficiency is lower than that of the planar one. This can be attributable to the higher area covered by PV cells in the planar LSC, which doubles the one of fiber LSCs. On the other hand, with normal incidence, there is also a higher efficiency when using square packed fibers because of the higher absorption efficiency with respect to hexagonal ones. Also, it can be

seen that the lower escaping losses of coated fibers compared with bulk-doped ones are balanced with their higher host absorption, resulting in similar efficiencies and concentration factors in both configurations. Additionally, as the fiber length is increased, optical efficiency decreases drastically while concentration factor stabilizes taking advantage of the high geometric factor, in the order of $10^3$. Also, because fiber LSC geometric factor doubles that of the planar one, the resulting $C_{oe}$ is now higher than in the planar case. However, due to the high impact of PLMA absorption at long lengths, LSC concentration factor barely reaches a value of 0.6 for bulk-doped PLMA fiber LSCs, showing the limitations in LSC performance caused by LSC host matrix absorption when fiber lengths reach several meters. Regarding diffuse source results, higher efficiency values are obtained at short lengths due to the scattering effect, which influenced beneficially, as either sunlight or luminescent light can be scattered directly to the solar cell. Also, the difference in performance between both packing types is fairly lower. In this case, bulk-doped PLMA fiber LSCs raise their concentration factor up to nearly 1.0, while it reaches around 1.5 for the coated PLMA fibers.
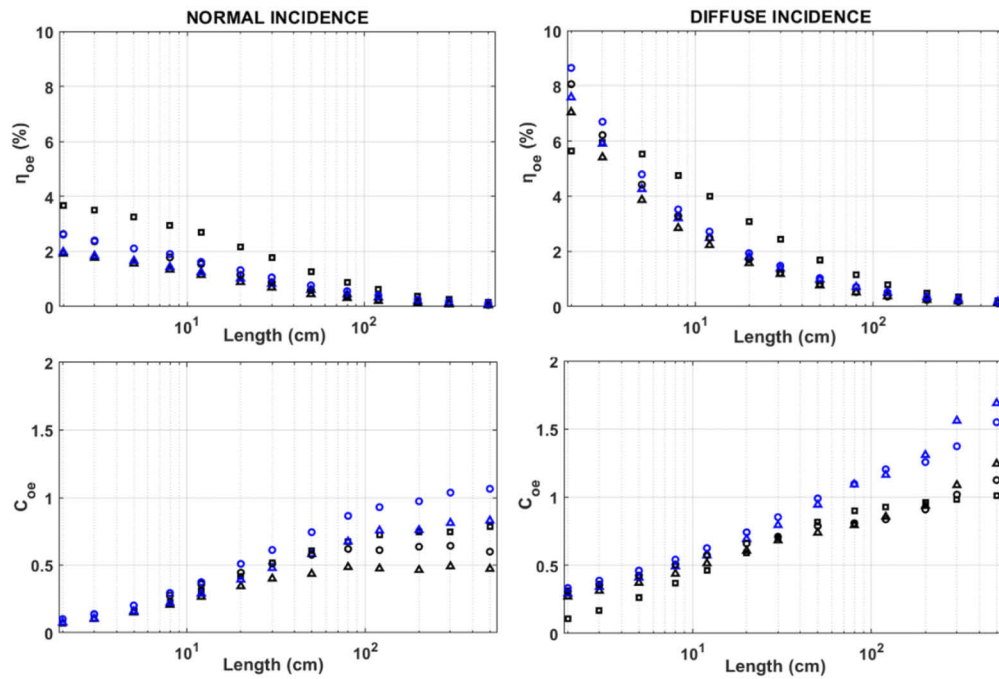


**Fig. 7.** Optical efficiency $\eta_{oe}$ and concentration factor $C_{oe}$ of radiant power as a function of the LSC length for bulk-doped (black) and coated (blue) PLMA fibers with an inner diameter of 30 μm and 3 μm of coating thickness arranged in hexagonal (triangle) and square (circles) packings for normal and diffuse incidence. Squares represent the values estimated from the LSC developed by Meinardi *et al.* [9].

## 5. Silica inner fiber

In this part, the same Si-QDs doped PLMA active coating is modelled while the PLMA waveguide core is replaced by ultra-low loss silica fibers. The core of the fibers, with an absorption coefficient $\alpha_{wg} \approx 10^{-4}$ cm$^{-1}$, is expected to provide a low loss path for re-emitted light guiding. This advantage may reduce the absorption losses, which limit large area LSCs performance.

The dopant concentration in the coating is increased to compensate the absorption reduction effect described in Fig. 5 and keep a similar light harvesting as in the planar LSC. As in the

previous case, different silica fiber diameters $D_{fiber}$ were studied while the $d/D_{fiber}$ ratio was fixed to 0.1. Figure 8 presents the resulting Si-QDs dopant concentrations calculated for different fiber diameters for hexagonal and square packings in order to make their absorption same as the planar LSC. As can be seen, the smaller the fiber diameter, the higher concentration is required, while also hexagonal packing needs a higher concentration. The highest dopant concentration is required for fibers with diameter of 30 μm and hexagonal packing with a value of 0.85 wt%, which is still much lower than concentrations reported in previous works. A recently published experimental work by Hill *et al.* [18] reported a noticeable high UV absorption of PLMA films doped with Si-QDs reaching concentrations as elevated as 3.3 wt% while avoiding significant quenching effects resulting from particle agglomeration at high doping concentrations. Also, such value is around 10 times greater than planar LSC concentration. This implies a change in the absorption coefficient at 480 nm from 1 cm$^{-1}$ to around 10 cm$^{-1}$ which yields according to Eq. (8), $\kappa \approx 0.0025$. Such value is much lower than one, so complex refractive index can be neglected. Despite the higher risk of quenching effects resulting from particle agglomeration at high doping concentrations, these effects are not considered in the model.
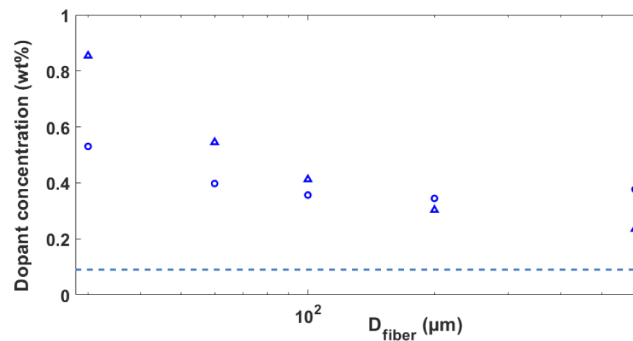


**Fig. 8.** Resulting Si-QDs dopant concentrations simulated for different fiber diameters for hexagonal (triangles) and square (circles) packings in order to equal the planar LSC absorption. Dashed line represents Si-QDs dopant concentration of 0.09 wt%, used in the planar LSC developed by Meinardi *et al.* [9].

Figure 9 presents the escaping, host, self-absorption and scattering losses as a function of the LSC length from 2 cm up to 5 m using silica coated fibers with diameters from 30 μm up to 600 μm and a normal incidence. When comparing escaping losses of silica core fibers with the coated PLMA ones from Fig. 6, similar values are predicted. Additionally, self-absorption losses slightly increase with respect to coated PLMA ones, as a result of the dopant concentration increase, which leads to a higher absorption at the wavelengths of re-emitted light. However, a marked decrease in host absorption losses can be noticed in silica fibers with respect to coated PLMA ones, since they are now lower than planar LSC ones, due to the low attenuation of the rays travelling along the low-loss core. Finally, a considerable increase of scattering losses is noticed in this case which approximate to values similar to those obtained for self-absorption, especially for hexagonal packed fibers with a diameter of 30 μm, due to the effects of the relatively high QD concentration used in this case.

As shown in Fig. 10, the former estimation of losses results in optical efficiencies of silica core fibers significantly higher than that of the coated PLMA ones (Fig. 7). As a result, it can be highlighted that the negative aspects of the $n_i < n_e$ configuration due to the higher probability of rays being confined in the coating, does not seem to be relevant compared with the effect of the reduction of the core absorption coefficient and, after all, the total balance is a reduction of the host absorption losses and the subsequent increase of the optical efficiency. Additionally, the
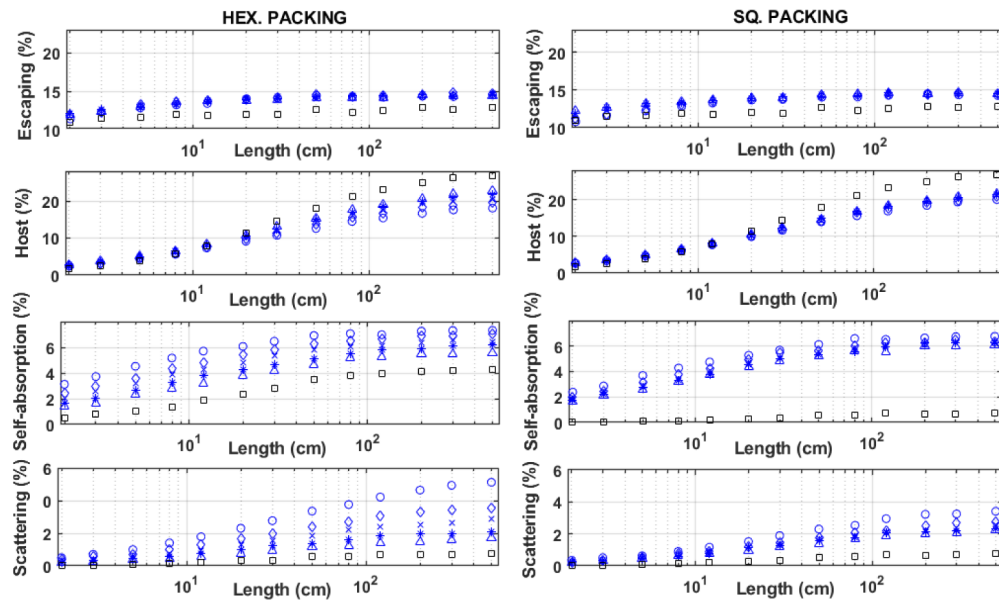
**Fig. 9.** The four sources of losses affecting photons after the first absorption/re-emission process as a function of the LSC length for coated silica fibers with diameters of 30 μm (circles), 60 μm (rombs), 100 μm (crosses), 200 μm (asterisks) and 600 μm (triangles) arranged in hexagonal (left) and square (right) packings calculated for normal incidence. Squares represent losses estimated from the LSC developed by Meinardi *et al.* [9].

scattering increase observed in Fig. 9 caused by the use of higher QD concentrations, does not have a significant contribution to penalize appreciably the LSC efficiency.

Regarding the concentration factor, no appreciable differences are observed when varying the fiber diameter for both types of incidence. On the other hand, in contrast with that of the planar LSC, the fiber one is seen to increase outstandingly and it becomes clearly greater at lengths of just a few tens of centimeters. This is due to the intrinsically higher geometric factor resulting from the fiber LSC design, which doubles the flat LSC one, and also, the higher optical efficiency favored by the lower escaping and host losses described above. When LSC dimensions become longer, the planar LSC concentration factor is seen to saturate at around 0.8 and 1.0, for normal and diffuse incidence, respectively, at LSC dimensions lower than 1 m². However, a better performance can be obtained from fiber LSC at larger dimensions as its concentration factor does not saturate until lengths of around 4 m. At these lengths, no further advantages can be taken from the geometric factor increase because the efficiency declines drastically due to the high host absorption losses resulting from the long path that the rays have to travel before being collected.

Finally, the concentration factor reveals a very remarkable outcome, since it reaches values of around 1.5 and 2.0, for normal and diffuse incidence, respectively, when dimensions are scaled over 1 m², which are more than 2 times the values of 0.8 and 1.0, reached for the planar LSC, and significantly higher than the values obtained for PLMA fibers, that lie between 0.5 and 1.0 for normal incidence and between 1.0 to 1.6 under diffuse conditions. This is more than twice the maximum concentration factor ever reported of 0.9 [11].
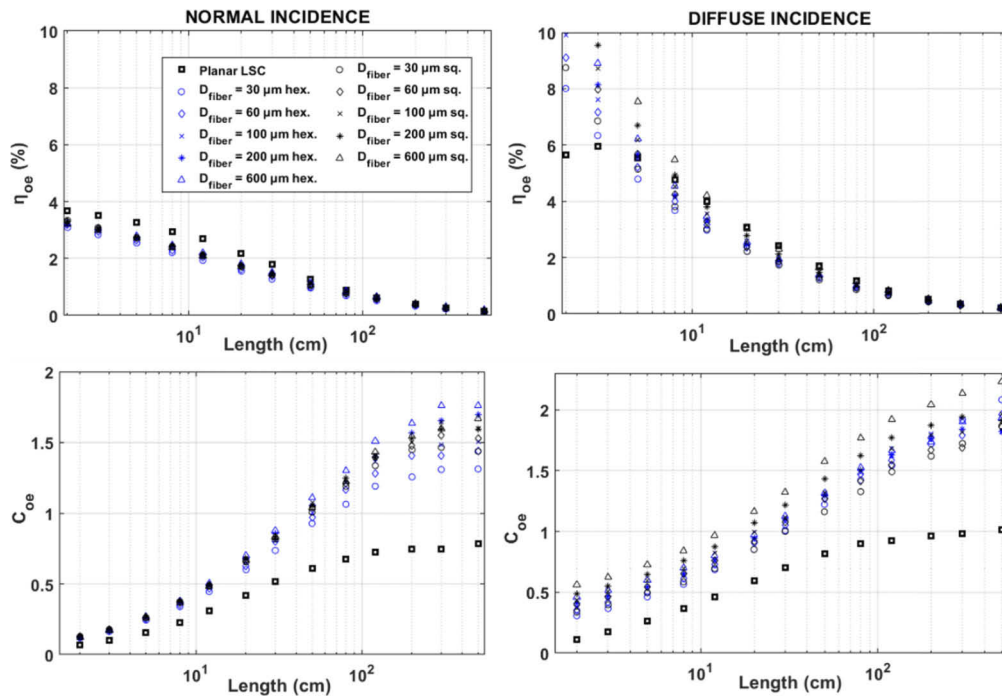
**Fig. 10.** Optical efficiency $\eta_{oe}$ and concentration factor $C_{oe}$ of radiant power for coated silica fibers with diameters of 30 μm (circles), 60 μm (rhombs), 100 μm (crosses), 200 μm (asterisks), 600 μm (triangles) arranged in hexagonal (blue) and square (black) packings for normal and diffuse incidence. Squares represent the LSC developed by Meinardi *et al.* [9].

## 6. Conclusions

In this work, a Monte Carlo simulation has been developed and validated to analyze the performance of a novel LSC design consisting of stacked layers of fiber arrays. The performance of different configurations of bulk-doped and coated fibers was compared against the conventional planar geometry while varying fiber packing geometry, diameter and length.

In the first part, a PLMA inner core was simulated and it was shown that, given the same amount of QDs, the fiber LSC absorbs a lower fraction of the incident light compared with that of the planar, being this effect more remarkable at lower diameters. Then, it was revealed that PLMA fiber LSCs concentration factor levels off at around 1 m², reaching a maximum value of of 0.7. At longer dimensions, no additional increase is appreciated, showing impact of the host absorption losses on LSC performance at longer dimensions.

Then, a silica based inner core was modelled instead, in order to provide a low-loss path for the guided fluorescent light and, as a result, a noticeable improvement of LSC concentration factor was obtained at meter-sized dimensions, which was shown to not saturate until lengths near to 4 m. Particularly, a maximum concentration factor of around 1.5 is obtained at normal incidence, in contrast with the values of 0.8 and 1.0, reached for the planar and the PLMA fiber LSCs, respectively. On the other hand, under diffuse conditions the concentration factor reaches a value around 2.0, which is far greater than the ones obtained for the PLMA-based LSCs, while also being more than twice the maximum concentration factor ever reported of 0.9.

These outstanding results serve as a stimulus for the development of meter-sized fiber LSCs based on stacked layers of silica micro-fibers coated with Si-QDs doped PLMA layers which

combine a high optical quality with excellent mechanical properties. These LSCs can be easily integrated as structural elements for façades or windows without interfering in the light spacing.

**Disclosures.** The authors declare no conflicts of interest.

**Supplemental document.** See Supplement 1 for supporting content.

## References

1. O. Morton, "A new day dawning?: Silicon Valley sunrise," Nature **443**(7107), 19–22 (2006).
2. M. A. Green, E. D. Dunlop, J. Hohl-Ebinger, M. Yoshita, N. Kopidakis, and X. Hao, "Solar cell efficiency tables (version 56)," Prog. Photovoltaics **28**(7), 629–638 (2020).
3. W. Shockley and H. J. Queisser, "Detailed balance limit of efficiency of p-n junction solar cells," J. Appl. Phys. **32**(3), 510–519 (1961).
4. W. H. Weber and J. Lambe, "Luminescent greenhouse collector for solar radiation," Appl. Opt. **15**(10), 2299–2300 (1976).
5. R. Mazzaro and A. Vomiero, "The Renaissance of Luminescent Solar Concentrators: The Role of Inorganic Nanomaterials," Adv. Energy Mater. **8**(33), 1801903 (2018).
6. B. McKenna and R. C. Evans, "Towards Efficient Spectral Converters through Materials Design for Luminescent Solar Devices," Adv. Mater. **29**(28), 1606491 (2017).
7. J. S. Batchelder, A. H. Zewai, and T. Cole, "Luminescent solar concentrators 1: Theory of operation and techniques for performance evaluation," Appl. Opt. **18**(18), 3090 (1979).
8. V. I. Klimov, T. A. Baker, J. Lim, K. A. Velizhanin, and H. McDaniel, "Quality Factor of Luminescent Solar Concentrators and Practical Concentration Limits Attainable with Semiconductor Quantum Dots," ACS Photonics **3**(6), 1138–1148 (2016).
9. F. Meinardi, S. Ehrenberg, L. Dhamo, F. Carulli, M. Mauri, F. Bruni, R. Simonutti, U. Kortshagen, and S. Brovelli, "Highly efficient luminescent solar concentrators based on earth-Abundant indirect-bandgap silicon quantum dots," Nat. Photonics **11**(3), 177–185 (2017).
10. F. Meinardi, H. McDaniel, F. Carulli, A. Colombo, K. A. Velizhanin, N. S. Makarov, R. Simonutti, V. I. Klimov, and S. Brovelli, "Highly efficient large-area colourless luminescent solar concentrators using heavy-metal-free colloidal quantum dots," Nat. Nanotechnol. **10**(10), 878–885 (2015).
11. S. F. H. Correia, P. P. Lima, E. Pecoraro, S. J. L. Ribeiro, P. S. André, R. A. S. Ferreira, and L. D. Carlos, "Scale up the collection area of luminescent solar concentrators towards metre-length flexible waveguiding photovoltaics," Prog. Photovoltaics **24**(9), 1178–1193 (2016).
12. Z. Krumer, S. J. Pera, R. J. A. Van Dijk-Moes, Y. Zhao, A. F. P. De Brouwer, E. Groeneveld, W. G. J. H. M. Van Sark, R. E. I. Schropp, and C. De Mello Donegá, "Tackling self-absorption in luminescent solar concentrators with type-II colloidal quantum dots," Sol. Energy Mater. Sol. Cells **111**, 57–65 (2013).
13. C. S. Erickson, L. R. Bradshaw, S. McDowall, J. D. Gilbertson, D. R. Gamelin, and D. L. Patrick, "Zero-reabsorption doped-nanocrystal luminescent solar concentrators," ACS Nano **8**(4), 3461–3467 (2014).
14. F. Meinardi, F. Bruni, and S. Brovelli, "Luminescent solar concentrators for building-integrated photovoltaics," Nat. Rev. Mater. **2**(12), 17072 (2017).
15. J. Roncali, "Luminescent Solar Collectors: Quo Vadis?" Adv. Energy Mater. **10**(36), 2001907 (2020).
16. S. K. E. Hill, R. Connell, C. Peterson, J. Hollinger, M. A. Hillmyer, U. Kortshagen, and V. E. Ferry, "Silicon Quantum Dot-Poly(methyl methacrylate) Nanocomposites with Reduced Light Scattering for Luminescent Solar Concentrators," ACS Photonics **6**(1), 170–180 (2019).
17. J. Huang, J. Zhou, T. Haraldsson, A. Clemments, M. Fujii, H. Sugimoto, B. Xu, and I. Sychugov, "Triplex Glass Laminates with Silicon Quantum Dots for Luminescent Solar Concentrators," Sol. RRL **4**(9), 2000195 (2020).
18. S. K. E. Hill, R. Connell, J. Held, C. Peterson, L. Francis, M. A. Hillmyer, V. E. Ferry, and U. Kortshagen, "Poly(methyl methacrylate) Films with High Concentrations of Silicon Quantum Dots for Visibly Transparent Luminescent Solar Concentrators," ACS Appl. Mater. Interfaces **12**(4), 4572–4578 (2020).
19. K. R. McIntosh, N. Yamada, and B. S. Richards, "Theoretical comparison of cylindrical and square-planar luminescent solar concentrators," Appl. Phys. B **88**(2), 285–290 (2007).
20. I. Sychugov, "Analytical description of a luminescent solar concentrator," Optica **6**(8), 1046–1049 (2019).
21. I. Sychugov, "Geometry effects on luminescence solar concentrator efficiency: Analytical treatment," Appl. Opt. **59**(19), 5715–5722 (2020).
22. G. Colantuono, A. Buckley, and R. Erdelyi, "Ray-Optics Modelling of Rectangular and Cylindrical 2-Layer Solar Concentrators," J. Lightwave Technol. **31**(7), 1033–1044 (2013).
23. K. Barnham, J. L. Marques, J. Hassard, and P. O'Brien, "Quantum-dot concentrator and thermodynamic model for the global redshift," Appl. Phys. Lett. **76**(9), 1197–1199 (2000).

24. A. J. Chatten, D. Farrel, C. Jermyn, P. Thomas, B. F. Buxton, A. Buchtemann, R. Danz, and K. W. Barnham, "Thermodynamic modelling of luminescent solar concentrators," in *Conference Record of the Thirty-First IEEE Photovoltaic Specialists Conference, 2005.* (2005), pp. 82–85.

25. D. Şahin, B. Ilan, and D. F. Kelley, "Monte-Carlo simulations of light propagation in luminescent solar concentrators based on semiconductor nanoparticles," J. Appl. Phys. **110**(3), 033108 (2011).

26. O. E. Semonin, J. M. Luther, and M. C. Beard, "Quantum dots for next-generation photovoltaics," Mater. Today **15**(11), 508–515 (2012).

27. O. Y. Edelenbosch, M. Fisher, L. Patrignani, W. G. J. H. M. van Sark, and A. J. Chatten, "Luminescent solar concentrators with fiber geometry," Opt. Express **21**(S3), A503–A514 (2013).

28. J. J. H. Videira, E. Bilotti, and A. J. Chatten, "Cylindrical array luminescent solar concentrators: performance boosts by geometric effects," Opt. Express **24**(14), A1188–A1200 (2016).

29. D. J. Farrell, "PVTRACE optical ray tracing for photovoltaic devices and luminescent materials," (2020).

30. "https://www.nrel.gov," https://www.nrel.gov/grid/solar-resource/spectra-am1.5.html.

31. Fedor Mitschke, *Fiber Optics*, 2nd ed. (Springer Berlin Heidelberg, 2016).

32. T. A. Germer, J. C. Zwinkels, and B. K. Tsai, "Chapter 2 - Theoretical Concepts in Spectrophotometric Measurements," in *Spectrophotometry*, T. A. Germer, J. C. Zwinkels, and B. K. Tsai, eds., Experimental Methods in the Physical Sciences (Academic Press, 2014), 46, pp. 11–66.

33. R. C. R. Barciela, F. Quintero, A. F. Doval, M. Fernández-Arias, J. del Val, and J. Pou, "Matlab Code for the Monte Carlo ray tracing model of a LSC based on stacked layers of fiber arrays with core-coating different absorbing properties," figshare, 2021 https://doi.org/10.6084/m9.figshare.14036105.